DYNAMIC INCREMENT OF PRESSURE ON UNDERGROUND RIGID WALL: COMPARING ANALYTICAL AND PHYSICAL MODELS

C. DAVIS [1], A. HUSHMAND [2], AND S. DASHTI[3]

[1]*Department of Water and Power, Los Angeles, CA, USA*
[2]*Hushmand Associates, Inc., Irvine, CA, USA*
[3]*Department of Civil, Environmental, & Arch. Engineering, University of Colorado Boulder, USA*

ABSTRACT

An analytical model is presented for evaluating the dynamic increment of lateral earth pressure on perfectly rigid unyielding walls. This solution is an extension of a previously published analytical model analyzing response of underground structures to vertically propagating waves. The structure is embedded in a deep viscoelastic soil. Wave propagation is determined from standard site response models. The soil is modeled as a continuum, and includes nonlinear behavior near the structure and in the far field. The analytical model is compared to dynamic increment of pressure on a very stiff underground structure for a 1 Hz sine input motion measured from centrifuge tests. The results show the analytical model compares well with the test measurements.

Keywords: rigid underground structure, dynamic increment of pressure, centrifuge test.

1. INTRODUCTION

The seismic response of underground structures is a complex soil-structure interaction problem dependent upon the properties of earthquake motions, surrounding soil, and structure. There are many different analytical and numeric models attempting to capture the complex dynamic soil and structure kinematic interactions. However, there are few good-quality tests for which to validate the models. Centrifuge tests were undertaken at the University of Colorado Boulder to improve the understanding of the physics underlying the underground structure behavior subjected to different types of ground motions. The results of these tests are used to make an initial comparison of an analytical model which evaluates underground rigid structures embedded in a viscoelastic soil medium subjected to vertically propagating seismic waves. This paper first presents the analytical model, then the physical model tested in the centrifuge, after which an initial comparison is made using a 1 Hz sine wave input motion.

2. ANALYTICAL MODEL

Figure 1 shows a model introduced by Davis (2003) used to develop a simplified analytical method to calculate dynamic earth pressures from propagating waves on the walls of a perfectly rigid-unyielding underground structure embedded in an infinite elastic half space. This model compared well to Wood (1973) and Veletsos and Younan (1994b) (Davis, 2003).

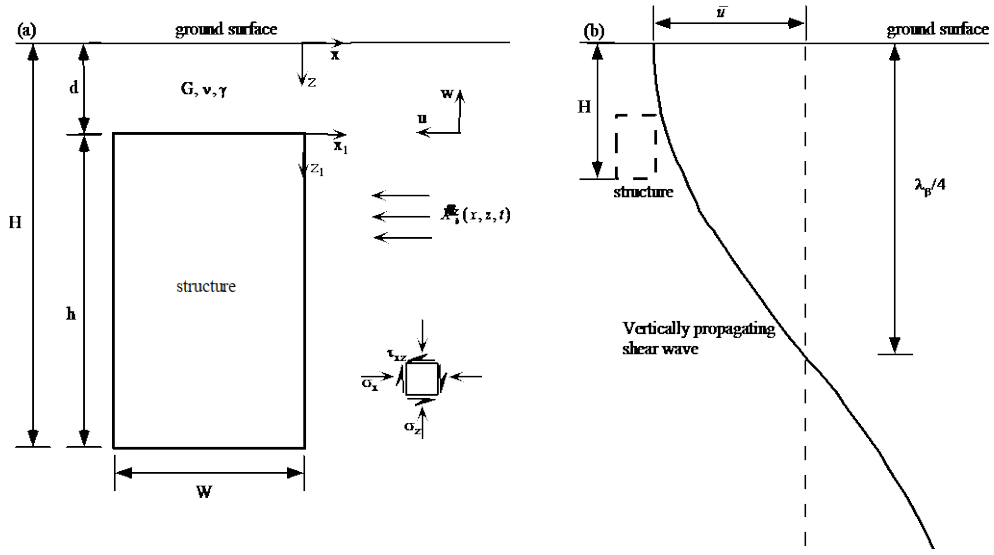

Figure 1: Davis (2003) underground rigid box structure model: a) structure geometry and coordinate systems, and b) wave propagation model at ground surface.

Figure 1a shows the model for evaluating lateral stresses on underground rigid box structures embedded within an infinite half-space. The half-space represents a deep unsaturated inhomogeneous, viscoelastic, soil deposit having a unit weight γ, shear modulus G, hysteretic damping ratio ξ, and Poisson ratio ν. γ, ξ, and ν are considered constant. The structure has a width W, vertical rigid walls of height h, and is buried a depth d with its base at depth H below the stress-free ground surface. The structure is assumed to have an infinite length L satisfying plain strain conditions. The model is defined by the x-z and x_1-z_1 coordinate systems originating at the ground surface and top of wall, respectively, which are related by $x = x_1$ and $z = z_1 + d$.

The structure is subjected to vertically incident shear waves. The horizontal and vertical motion in the soil medium is represented by displacements u and w, respectively, having positive motions as defined in Fig. 1a. Figure 1a also shows the stress sign convention where compressive stresses are defined as positive. The dynamic increment of earthquake pressure σ_x is given by:

$$\sigma_x = k_s u = k_s (u_f - u_H) \qquad d \le z \le H \tag{1}$$

Davis (2003) also proposed a lateral stress increase with soil densification $\Delta\sigma_h$, which will not be addressed in this paper. In Eq. 1, k_s is a continuous soil stiffness parameter, u is the horizontal displacement function, u_f is the horizontal soil free-field deformation during seismic shaking, u_H is the horizontal soil free-field deformation at depth H. The closed form analytical solution using elastic wave propagation theory is presented in Davis (2003) and only some of the results will be summarized herein. The horizontal displacement is given by:

$$u = \bar{u}\left(1 - e^{-k_\beta x_1/\psi_e}\right)\left(\cos k_\beta (z_1 + d) - \cos k_\beta H\right), \quad \psi_e^2 = \frac{2-\nu}{1-\nu}, H \le \lambda_\beta/4 \tag{2}$$

where $\bar{u}$ is the horizontal free-field displacement at the ground surface, λ_β is the shear wave length, $k_\beta = \omega/\beta$ is the shear wave number, $\omega = 2\pi f$ is the angular frequency, f is the wave frequency, β is the free-field shear wave velocity of the soil. The harmonic nature of the motion described by $e^{-i\omega t}$ is implied in Eq. 2 and subsequent functions.

The Davis (2003) model assumed the soil stiffness varied with depth but G in the wall vicinity and in the free field are modified similarly with the applied free field shear strain (i.e. G was constant for all x at any depth z). However, the free field and near-wall strains are not equal and thus the model presented herein improves the ability to more accurately estimate the soil stiffness using the shear modulus G_{xz}, which is not a constant value but varies primarily as a function of void ratio, relative density, plasticity index, mean effective pressure, shear strain, and number of shearing cycles (Bardet, 1997; Hardin and Drnevich, 1972; Ishibashi and Zhang, 1993).

In the free-field, the initial small strain shear moduli $G_i^* = G_i /(1+2i\xi)$, in the absence of seismic shaking, is determined at any depth z from:

$$G_i^* = G_0(1+2i\xi) f_G(z), \quad f_G(z) = (z/H)^m \tag{3}$$

where $G_0 = G_0^*/(1+2i\xi)$ is the reference free-field small strain modulus at depth H, and $f_G(z)$ is a function representing the variation in shear moduli with depth. The inhomogeneity coefficient m varies as a function of plasticity index and shear strain amplitude (Ishibashi and Zhang, 1993); the value of m typically ranges from ½ for small strains to 1 at large strains (Hardin and Drenovich, 1972; Bardet, 1997). When a seismic shear strain is applied the shear modulus varies as:

$$G_{xz} = \Omega_{xz} G_0 f_G(z) \tag{4}$$

Ω_{xz} is a coefficient defining how G_{xz}/G_0 varies with shear strain (e.g., Ishibashi and Zhang, 1993) at a specified depth. The shear strain function, presented in Eq. 8 below, varies with x_1 and z and becomes that of the free-field (i.e., independent of x_1) at approximately $x_1 = 3h$, where $\Omega_{xz} = \Omega_{fz}$. Thus, Ω_{xz} is a continuous function varying from Ω_{sz} at $x_1 = 0$ to Ω_{fz} at $x_1 = 3h$ for a given depth. Using this notation, the shear modulus can be defined at any x and z coordinate, where the subscripts s and f indicate the shear modulus at the structure or in the free-field, respectively, and the subscript H indicates the reference modulus at depth $z = H$.

The soil stiffness parameter at $x_1 = 0$ is:

$$k_s = \frac{2G_{sz}k_\beta}{\sqrt{(1-\nu)(2-\nu)}} = G_{sz}k_\beta\psi_\sigma, \quad \psi_\sigma = \frac{2}{\sqrt{(1-\nu)(2-\nu)}} \tag{5}$$

The free-field shear wave velocity of the soil medium is:

$$\beta = \sqrt{gG_{fH}/\gamma}\left(\frac{z}{H}\right)^{\frac{m}{2}} = \sqrt{g\Omega_{fH}G_o/\gamma}\left(\frac{z}{H}\right)^{\frac{m}{2}} \tag{6}$$

where g is the acceleration of gravity. β_0 is the small strain shear wave velocity associated with $G_{fH} = G_0$ (i.e., $\Omega_{fH} = 1$). At depth H the reference shear wave velocity is $\beta = \sqrt{gG_{fH}/\gamma}$.

The free field displacements u_f for $H \geq z \geq 0$ defined by Davis (2003) as $x_1 \geq 3h$, are given by:

$$u_f = \bar{u}\left(\cos 2\pi \frac{z_1 + d}{\lambda_\beta} - \cos\frac{2\pi H}{\lambda_\beta}\right) \tag{7}$$

The shear strain ε_{xz} and shear stress τ_{xz} are given by:

$$\varepsilon_{xz} = \bar{u}k_\beta^2\left\{\left(1 - \frac{2}{\psi_e^2}e^{-k_\beta x_1/\psi_e}\right)\frac{1}{k_\beta}\sin k_\beta(z_1 + d) - \frac{\nu}{2-\nu}e^{-k_\beta x_1/\psi_e} z\cos k_\beta H\right\} \text{ and } \tau_{xz} = G_{xz}\varepsilon_{xz} \tag{8}$$

Substituting Eqs. 3 to 8 into Eq. 1 at $x_1 = 0$ gives:

$$\sigma_x = \frac{\bar{u}\gamma}{g}\frac{\Omega_{sH}}{\sqrt{\Omega_{fH}}}\psi_\sigma\beta_0\omega\left(\frac{z_1 + d}{H}\right)^m\left[\cos\left(\frac{2\pi f}{\beta}(z_1 + d)\right) - \cos\left(\frac{2\pi f}{\beta}H\right)\right] \tag{9}$$

where σ_x is the compressive stress against the structure. Equation 9 shows the lateral stresses applied to the structure are dependent upon the frequency of input motion because of the soil stiffness parameter in Eq. 5. The stress amplitude in Eq. 9 is independent of frequency when the velocity amplitude $\bar{v} = -\bar{u}\omega$ is substituted for $\bar{u}$.

Motions are usually made up of multiple waves of different frequency f_p, where p is the number of wave frequencies making up the motions striking at the same time. For these compound motions the stress on the wall is a result of the superposition of displacements from each wave of frequency f_p.

Equations 2, 5, and 9 (substituting $|\bar{v}|$), respectively, become:

$$u = \bar{u}\sum_p \frac{a_p}{\sum_p a_p}\left(1 - e^{-k_{\beta p}x_1/\psi_e}\right)\left(\cos k_{\beta p}(z_1 + d) - \cos k_{\beta p}H\right) \tag{10}$$

$$k_{sp} = \frac{2G_{sz}k_{\beta p}}{\sqrt{(1-\nu)(2-\nu)}} = G_{sz}k_{\beta p}\psi_\sigma \tag{11}$$

$$\sigma_x = \frac{\bar{v}\gamma}{g}\frac{\Omega_{sH}}{\sqrt{\Omega_{fH}}}\psi_\sigma\beta_0\left(\frac{z_1 + d}{H}\right)^m S, S = \sum_p \frac{a_p}{\sum_p a_p}\left[\cos\left(\frac{2\pi f_p}{\beta}(z_1 + d)\right) - \cos\left(\frac{2\pi f_p}{\beta}H\right)\right] = \frac{u(z)}{\bar{u}} \tag{12}$$

Where a_p is the Fourier coefficient for wave p of frequency f_p. The shape function S is derived from the Eq 10 free field motion.

3. PHYSICAL MODEL

Dynamic tests of model buried structures were performed at 60g of centrifugal acceleration using the 5.5 m-radius, 400 g-ton geotechnical centrifuge at the University of Colorado Boulder. The model specimens were prepared in a flexible shear beam (FSB) container (Ghayoomi et al. 2013).

The response of the system during testing was measured using 27 accelerometers, 8 LVDTs, 16 strain gauges (8 on each wall), 4 tactile pressure transducers (2 on each wall), and 16 earth pressure cells (8 on each wall). The location of the transducers is shown in Figure 2. Each tactile sensor contains 14 rows and 14 columns of sensels (sensing points) amounting to 196 sensels, each 5.1 mm by 5.1 mm. Each of the 196 sensels recorded pressure data at a rate of 4,000 samples/sec during the dynamic centrifuge tests.

Dry Nevada sand No. 120 (G_s=2.65; e_{min}=0.56; e_{max}=0.84; D_{50}=0.13 mm; C_u=1.67) was pluviated in the FSB container at a target relative density of D_r=60% (γ_d=15.6 kN/m^3). The soil deposit was dry pluviated in layers using a hopper at a calibrated height to achieve the target D_r. The total soil depth D = 18.7m.

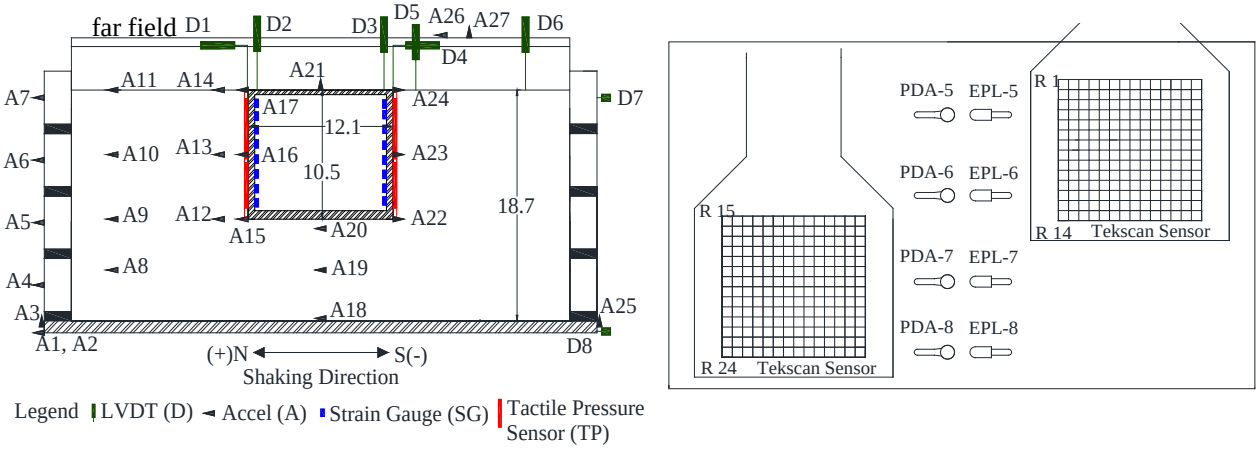

Figure 2. Left: Instrumentation layout of a representative centrifuge test (dimensions shown in prototype scale meters). Right: Pressure sensor layout on each wall of the buried structure.

The model structures were designed based on a simplified version of prototype reservoir structures by maintaining a similar natural frequency and lateral stiffness (detailed by Hushmand et al. 2016). The model structure was constructed of four pieces of welded 1018 Carbon Steel (density = 7870 kg/m^3; Young's modulus = 2×10^8 kPa). The structure dimensions are: outer height = 10.5 m, outer width = 12.1 m, base thickness = 1.46 m, roof thickness = 1.12 m, and wall thickness of 1.13 m. The fundamental frequency was experimentally and numerically calculated at 9 to 10 Hz.

Ground motions were applied to the model specimens in flight using the servo-controlled, electro-hydraulic shake table (Ketcham et al. 1991) mounted on the basket at the end of the centrifuge arm. A series of five horizontal earthquake motions and eight sinusoidal motions (15 cycles) were applied to the base of the model specimen, in the order listed in Table 1. The amplitude of sinusoidal motions was kept about the same, while their frequencies were varied.

Table 1. Achieved base motion characteristics (prototype scale)

	Input motion parameters			
Shaking Event	PGA (g)	I_a (m/s)	$D_{5\text{-}95}$ (s)	f_m (Hz)
Northridge-L	0.30	1.42	21.14	1.2
Northridge-M	0.66	4.49	24.2	1.35
Northridge-H	1.0	9.0	27.0	1.45
Izmit	0.34	1.8	40.50	---
Sine 0.33 Hz	0.32	---	15	---
Sine 1 Hz	0.32	---	15	---
Sine 2 Hz	0.34	---	15	---
Sine 3 Hz	0.36	---	15	---
Sine 4 Hz	0.34	---	15	---
Sine 5 Hz	0.47	---	15	---
Sine 6 Hz	0.34	---	15	---
Sine 6.7	0.44	---	15	---
Loma	0.97	9.61	13.30	1.96

The test procedures and results are provided in Hushmand (2016) and HAI (2016). The physical and analytical models are compared using the sine 1 Hz motion and pressures on the north wall, which is assumed to approximate a perfectly rigid structure.

4. COMPARISON

The sine 1 Hz acceleration time histories were integrated to obtain velocity and displacement series. These were baseline corrected with a cubic polynomial and filtered using a 6th order Butterworth bandpass between 0.3 and 25 Hz. The displacement time series required an additional linear baseline correction. The surface far-field motions and Fourier spectra at A11 are shown in Fig. 3. The small strain shear wave velocity was obtained by evaluating the pre-shaking recorded noise, identifying the site natural frequency of 6 Hz, and calculating $\beta_0 = 4 f_0 H_{site}$ = 450m/s. The dynamic increment of pressure was estimated as the difference between the total and preshake, static lateral earth pressure for the sine 1 Hz recording. The recorded data was pre-processed to reduce scatter as described in Hushmand et al. (2016b).

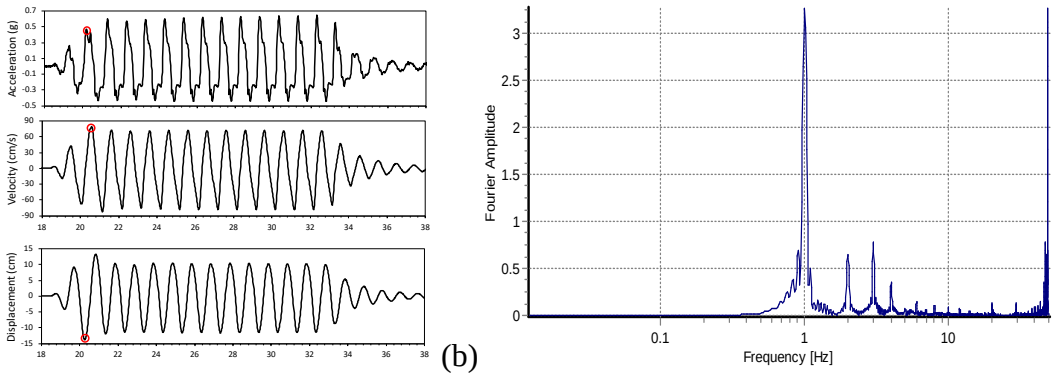

Figure 3. (a) Acceleration, velocity, and displacement time histories recorded at A11. Circles represent values at time used for comparing models. (b) Fourier spectra for records in (a).

The lateral pressures are evaluated at time of greatest negative displacement having 13.7 cm, identified in Fig. 3, which is associated with a peak particle velocity of 79.1 cm/s, and acceleration 0.43g. Negative displacements apply pressure to the north wall. Figure 4a shows the shape function estimated for site response for a rigid base, as shown in Fig. 2, compared to displacement ratios in the far field measured at A8 to A11. The estimated response used S from Eq. 12 with Fourier coefficients shown in Fig. 3b for frequencies 1 to 8 Hz. The far field β = 170m/s used to calculate S was estimated by measuring the average time for peak displacements, velocities, and accelerations to propagate between each station bounding the structure base elevation. As seen in Fig. 4a, the estimated and measured shape functions compare very well.

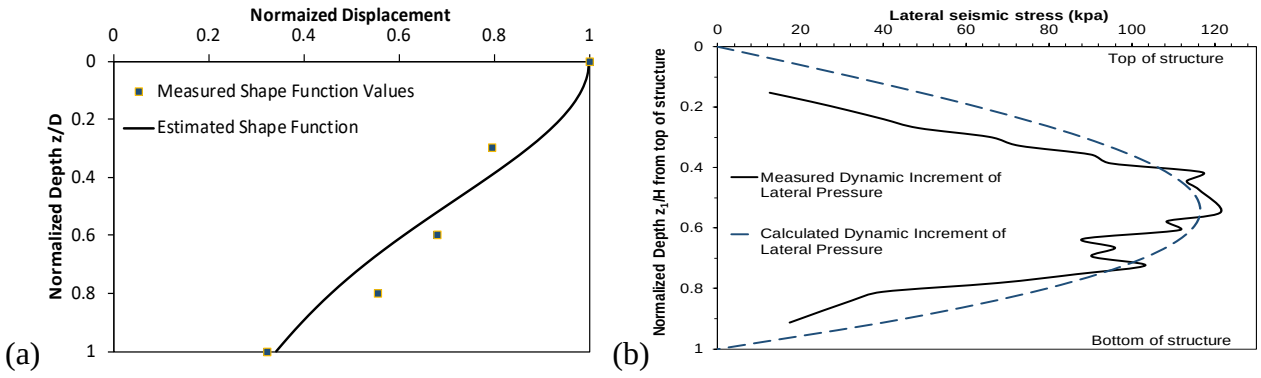

Figure 4. (a) Shape Function. (b) Comparison of dynamic increment of soil pressure.

Strains were calculated between each adjacent set of far field recordings between A2 and A11 and also near structure recordings A12 to A14. Strains in the far field at structure base elevation are approximately 0.004 to 0.007 at time of peak displacement, and near structure base strains were about 0.003 to 0.004 at same time. The soil shear strains at near structure are slightly larger than those at the structure and the far field strains are lower than the theoretical free field. The measured strains can be adjusted by use of Eq. 8 to the expected values. Theoretically the far field strains measured at $x = 1H$, shown in Fig. 2, are smaller than free field shear strains occurring at $x = 3H$. However, the FSB has some level of influence on the test results. Since the shape function matches closely with the measured values, the FSB is believed to be approximately equal for the far field to free field strains and the displacements, and therefore no adjustments are made to estimate free field strains. The strains at structure are about 77% of those measured at near-structure. The strain values result in Ω_{sH} = 0.53 and Ω_{fH} = 0.33 using the formulation for G/G_0 of Ishibashi and Zhang (1993).

Figure 4b shows the measured dynamic increment of pressure and that calculated using Eq. 12 using the parameters described above and d = 0, ν = 0.3, γ = 15.9kPa. The value of γ is based on initial unit weight described in Hushmand et al. (2016a) and the increase in value from settlement presented in Hushmand et al (2016b). The damping ratio is not needed for the calculation since the wave solution is based on measured surface motions. Figure 4b shows the increment of dynamic pressure calculated from Eq. 12 using measured values compares very closely with the recorded pressures. This indicates the analytical model can be applied for the soil parameters used in the

physical model at a 1 Hz frequency. The comparison needs to be extended to other frequencies and additional tests to confirm its usefulness for a wide range of conditions.

5. CONCLUSIONS

The proposed analytical model compares very well with the measured dynamic increment of pressure for the sine 1 Hz input motion. This indicates the most important parameters describing the basic physics of the underground soil-structure interaction problem as tested are incorporated into the analytical model. Additional comparisons are necessary to fully validate the analytical model.

6. ACKNOWLEDGMENTS

The Los Angeles Department of Water and Power is acknowledged for support of this work.

REFERENCES

Bardet, J.P. (1997) "*Experimental Soil Mechanics*," Prentice-Hall, N.J.

Davis, C. A.**,** 2003, "Lateral Seismic Pressures for Design of Rigid Underground Structures, *Proc. 6th U.S. Conf. on Lifeline* Earthquake *Engineering, Monograph 25,* ASCE, Long Beach, Aug., 10-13, pp. 1001-1010.

Ghayoomi, M., Dashti, S., & McCartney, J. S. (2013). "Performance of a transparent Flexible Shear Beam container for geotechnical centrifuge modeling of dynamic problems". *Soil Dynamics and Eqk. Engineering, 53,* 230-239

Hardin, B. O., and V. P. Drnevich, 1972, "Shear Modulus and Damping in Soils: Measurements and Parameter Effects," *Journal of the Soil Mechanics and Foundations Division*, ASCE, Vol. 98, No. SM6, pp. 603-624.

Hushmand, (2016). Seismic Performance of Underground Reservoir Structures. Ph. D. Thesis, Department of Civil, Environmental, and Architectural Engineering, University of Colorado, Boulder.

Hushmand and Associates, Inc. (2016). Geotechnical Centrifuge Modeling of Seismic Response of Underground Reservoir Structures. Data Report prepared for Los Angeles Dept. of Water and Power.

Hushmand, A., S. Dashti, C. Davis, B. Hushmand, M. Zhang, M. Ghayoomi, J.S. McCartney, Y. Lee, and J. Hu (2016a). "Seismic Performance of Underground Reservoir Structures: Insight from Centrifuge Modeling on the Influence of Structure Stiffness," *ASCE J.G.G.E.., 10.1061/(ASCE)* GT.1943-5606.0001477, 04016020.

Hushmand, A., S. Dashti, C. Davis, B. Hushmand, Y. Lee, and J. Hu, 2016b, "Seismic Performance of Underground Reservoir Structures: Insight from Centrifuge Modeling on the Influence of Backfill Soil Type and Geometry," *ASCE J. Geotech. Geoenviron. Eng., 10.1061/(ASCE)* GT.1943-5606.0001544, 04016058.

Ishibashi, I, and X. Zhang, 1993, "Unified Dynamic Shear Moduli and Damping Ratios of Sand and Clay," *Soils and Foundations*, Japanese Society of Soil Mechanics and Foundation Engineering, Vol. 33, No. 1, pp. 182-191.

Ketcham, S. A., Ko, H. Y., and Sture, S. (1991). ''Performance of an earthquake motion simulator for a small geotechnical centrifuge.'' *Centrifuge 91*, H. Y. Ko and F. G. McLean, eds., Balkema, Rotterdam, The Netherlands, 361–368.

Richards, R. Jr., C. Huang, and K. L. Fishman (1999) "Seismic Earth Pressure on Retaining Structures," *Journal of Geotechnical and Geoenvironmental Engineering*, ASCE, Vol. 125, No. 9, pp. 771-778.

Scott, R. F. (1973) "Earthquake-Induced Pressures on Retaining Walls," *Proc., 5th World Conf. On Earthquake Engr.*, Int. Assn. of Eq. Engrg., Tokyo, 2, 1611-1620.

Veletsos, A. S., and A. H. Younan (1994a) "Dynamic Soil Pressures on Rigid Vertical Walls," *Earthquake Engineering and Structural Dynamics*, Vol. 23, pp. 275-301.

Veletsos, A. S., and A. H. Younan (1994b) "Dynamic Modeling and Response of Soil-Wall Systems," *J. Geo. Engr.*, ASCE, Vol. 120, No. 12, pp. 2155-2179.

Wood, J. H. (1973) "Earthquake-Induced Soil Pressures on Structures," Report EERL 73-05, Earthquake Engr. Research Laboratory, California Institute of Technology.